Weakly Interacting Molecular Spins in On-Surface Synthesized Nanoclusters on a Graphene Oxide Nanosheet

Makoto Sakurai, Tsuyoshi Ueta, Christian Joachim

Spin liquid-like behavior of weakly interacting molecular spins in nanoclusters on a graphene oxide nanosheet

Weakly interacting molecular spins in on-surface synthesized nanoclusters on a graphene oxide nanosheet

Makoto Sakurai,[1] Tsuyoshi Ueta*[2] and Christian Joachim[1,3]

1 International Center for Materials Nanoarchitectonics (WPI-MANA), National Institute for Material Sciences (NIMS), 1-1 Namiki, Tsukuba, Ibaraki 305-0044, Japan
2 Jikei University School of Medicine, 8-3-1 Kokuryo, Chofu, 182-0022, Japan.
3. Centre d'Elaboration de Matériaux et d'Études Structurales (CEMES), Centre National de la Recherche Scientifique (CNRS), 29 Rue J. Marvig, BP 4347, 31055 Toulouse Cedex, France.

E-mail: sakurai.makoto@nims.go.jp

With an average diameter of about 2 nm, on-surface synthesized amino-ferrocene nanoclusters are chemisorbed onto a graphene oxide nanosheet, where their Fe ions are in an S = 5/2 high-spin state. In this two-dimensional (2D) nanomaterial, the molecular spins in a given nanocluster are weakly magnetic dipole interacting. It generates spin correlations and slow dynamics accessible by magnetic susceptibility and Mössbauer spectroscopy at a temperature where the magnetic anisotropy is negligible. Magnetic simulations show that minimizing their magnetic dipole energies produces spatially entangled structures of the spin orientations at $T \lesssim 15$ K and that the structures behave like a spin liquid. The competition between the formation of the structures and their thermal destruction generates the slow dynamics. The ability to create emergent functionalities from dense stacks of weakly interacting magnetic molecules in a 2 nm space paves the way for new designs of an ultra-compact building block and a functional component in 2D spintronic and neuromorphic devices.

1. Introduction

Engineering the magnetic interactions between molecular spins plays an essential role in the chemical design and arrangement of molecular magnets, magnetic molecules, and their assemblies required for the integration of nanoscale spintronic and neuromorphic devices. On the one hand, molecular magnets have the ability to maintain the spin orientations through magnetic anisotropy and intramolecular exchange interactions,[1,2] and a variety of magnets

have been synthesized for molecular spintronics and quantum computing, acting as information storage devices [3,4] and, for those with long spin coherence, as building blocks for quantum computation.[5,6] Some magnetic molecules have another ability to self-assemble into various nano- and micro-scale structures,[7,8] which can lead to the development of new functionalities not accessible to single molecules through structuring in combination with the intrinsic properties of the molecules themselves. The amino-ferrocene molecules used in this study (**Figure 1**A) can self-assemble into nanoclusters on a graphene oxide nanosheet via on-surface chemical reaction.[9] We have measured the magnetic properties dense stacked weakly interacting molecular spins into a nanocluster with a diameter of about 2 nm and discussed those properties by combining theoretical simulations and a systematic analysis of the experimental data.

The amino-ferrocene-based assemblies, referred to as nanoclusters in this study, are chemisorbed on the surface of a graphene oxide (GO) nanosheet, forming a 2D material. The electronic states of the 3d electrons of the Fe ion in ferrocene or ferrocene-derivatives are dominated by the ligand field.[10] Inside the nanocluster, the Fe ion of a given amino-ferrocene molecule has unpaired electrons due to the through-bond electron transfer process between the Fe ion and the GO,[9] which behaves as a localized spin due to the geometry of the ferrocene unit (Figure 1A). Magnetic dipole interactions between localized spins in molecular assemblies are generally much weaker than intramolecular interactions and magnetic anisotropy in the molecule, because the dipole energy approximated as m^2/r^3 is equivalent to only 0.0006 K assuming a magnetic moment m of 1 μ_B and a distance r between them of 1 nm. However, in assemblies of small magnets with large magnetic moments, magnetic dipole interactions have been reported to play a crucial role, for example, in the magnetic ordering in high-spin molecular cluster magnet crystals [7-8] and in the modulation of magnetic relaxation in magnetic nanoparticle assemblies.[11,12] Here, the nearest dipole interactions dominate mainly the formation of these properties. In our amino-ferrocene-based nanoclusters, the d_m = 0.28 nm distance between neighboring localized spins[9] (Figure 1A) is much shorter than the d_m between neighboring magnetic moments in Fe_{12} cluster magnet crystals ($d_m \approx 1.4$ nm) [7] and in nanoparticle assemblies (d_m = 2 – 10 nm) [11,12], leading to the completely different situation that all molecular spins within the nanocluster are weakly connected by magnetic dipole fields of the order of 10^2 - 10^3 Oe. The interactions in the nanoclusters differ from that treated in a mean-field-based theory.[13] In addition, the controlled on-surface self-organization of our nanoclusters can produce a uniform nanocluster distribution with a relatively large inter-cluster distance,[9] resulting in a surface structure close to an isolated

magnetic nanocluster distribution on an insulating GO nanosheet. Here, we analyze the behavior of dense packed molecular spins resulting from such unique magnetic interactions in nearly zero-dimensional nanoclusters by measuring the magnetic susceptibility, magnetization, ^{57}Fe Mössbauer spectrum, and by simulating the distribution of the spin orientations by Markov-chain Monte Carlo methods. We also elucidate the mechanism of the slow dynamics generated in this 2D material by comparing it with that studied in spin glasses [14,15], interacting magnetic nanoparticles [11,12], and frustrated magnets [16,17].

2. Results and Discussion

The deviation from the paramagnetic Fe ions in the amino-ferrocene (AFc) molecules forming the nanoclusters on a GO nanosheet (AFc-GO sheets) was estimated by accounting static magnetization and magnetic susceptibility. On the GO nanosheets and resulting in an average inter-cluster distance $\langle d \rangle$ of 10 nm (Figure 1A), the amino-ferrocene-based nanoclusters were synthesized for 5 hours by our on-surface chemical reaction technique (Methods).[9] The small black spots in a transmission electron microscope (TEM) image (Figure 1B) and small white spots in a scanning transmission microscope (STEM) image (Figure S1, Supporting Information) of a chemically reacted GO nanosheet correspond to amino-ferrocene-based nanoclusters on a GO nanosheet (Figure S1, Supporting Information). The diameter distribution of the AFc-GO sheets ($\langle d \rangle$ = 10 nm) shows an average diameter of about 2 nm (Inset of Figure 1B). As calculated from the magnetization of the AFc-GO sheets and of the pristine GO nanosheets,[9] the magnetization M_{AFc} of the molecules on the GO nanosheets is plotted in Figure 1b as a function of $\mu_{\mathrm{B}}H/k_{\mathrm{B}}T$, where μ_{B} is the Bohr magneton, H is the applied magnetic field, k_{B} is the Boltzmann constant, and T is the temperature. Characterizing the paramagnetic properties of a material as a function of field and temperature,[18] the Brillouin $B_{\mathrm{S}}(\mu_{\mathrm{B}}H/k_{\mathrm{B}}T)$ and Langevin $L_{\mathrm{S}}(\mu_{\mathrm{B}}H/k_{\mathrm{B}}T)$ functions are plotted as solid and dotted lines using the spin state numbers S = 5/2 or S = 1/2 (Figure 1C and Figure S2, Supporting Information), respectively. At small $\mu_{\mathrm{B}}H/k_{\mathrm{B}}T$ values, the experimental data are well fitted using S = 5/2. However, at low temperature and high field, the experimental data deviated from the lines meaning that a change in the energy levels of the 3d electrons under the applied field is not expressed simply by the Zeeman splitting,[18] as $\mu_{\mathrm{B}}H/k_{\mathrm{B}}T$ increases. This is different from superparamagnetic materials for example ferromagnetic nanoparticles[19] and molecular magnets.[20,21] Note that this deviation was observed at T = 50 and 100 K,

where the thermal energy is certainly larger than the magnetic interactions between the neighboring Fe ions.

Under a small magnetic field and for T > 20 K, the static susceptibility $\chi_{\mathrm{M,AFc}}$ of our nanomaterial follows the Curie-Weiss law:[18] $\chi_{\mathrm{M,AFc}} = C/(T-\Theta)$ (Figure 1D). The constant $C = g^2\mu_B^2 S(S+1)/3k_{\mathrm{B}}W_{\mathrm{FD}}$ [18] is the slope of a linear fit to the experimental data, where g is the g-factor and W_{FD} is the mass of the molecule. Assuming g = 2, C gives a magnetic moment $g\mu_{\mathrm{B}}S$ = 5.1 μ_{B}, confirming that the Fe ions are in the high-spin state (S = 5/2) rather than the low-spin state (S = 1/2) (Figure 1A). Note that this value was underestimated in our previous study[9] because it was determined in a magnetic field of 70 kOe and in an unsaturated *M-H* loop at T = 2 K. The constant Θ was -2.9 K, indicating that there were negative interactions, as predicted by mean-field theory.[18]

Low-temperature zero-field ^{57}Fe Mössbauer spectroscopy[22,23] confirms that the Fe ion in the amino-ferrocene molecules changed from a non-magnetic S = 0 state to a S = 5/2 high-spin state when assembled by on-surface chemical reaction on a GO nanosheet. At 5 K, the Mössbauer spectrum of a pristine amino-ferrocene powder indicated that the Fe ions here are in the Fe^{2+} S = 0 nonmagnetic state (**Figure 2**A).[11] On the other hand, for the amino-ferrocene molecules assembled on a GO nanosheet surface, a magnetic hyperfine splitting was clearly seen in the spectra (Figure 2B). This is due to the change in the ionized state of the Fe ions caused by the charge transfer.[9] As the temperature increased, thermal disturbances attenuated the peaks in the spectra. The onset temperature to observe a splitting was about 15 K and the separation between the peaks did not depend on temperature (Figure 2B). This is different from the splitting temperature dependence observed for superparamagnetic particles whose magnetic properties are dominated by magnetic anisotropy.[24] At 5 K, the parameters characterizing the 3d electrons in the Fe ions were determined by taking the best fit of the spectrum (Figure S3, Supporting Information). As summarized in Table S1 (Supporting Information) and at 5 K, the 470 - 400 kOe hyperfine magnetic fields for an AFc-GO sheet again confirm that the Fe ions are in an S = 5/2 Fe^{3+} high-spin state and not in the S = 1/2 low spin state.[22] At 5 K, about 82% of the Fe ions on the AFc-GO sheets have a large hyperfine field corresponding to S = 5/2. About 18% of the Fe ions on the GO nanosheets are in the S = 0 non-magnetic state. Some of the amino-ferrocene molecules have not chemically reacted with the GO surface and do not contribute to the magnetic properties of the chemically reacted sheets.

Magnetic properties of a mononuclear organometallic molecule are generally characterized by a magnetic anisotropy resulting from zero-field splitting at its metal site.[25] There are few experimental reports on the magnetic anisotropy of ferrocene molecules because individual ferrocene molecules do not have unpaired 3d electrons.[11] Assembled on a GO nanosheet, Fe^{3+} ion 3d electrons are in a high $S = 5/2$ spin state and the electronic cloud of the 3d electrons is spherically distributed (no orbital-angular momentum).[26] Therefore, the spin-orbit interactions normally at the origin of magnetic anisotropy are too small to produce the hyperfine splitting observed in the Mössbauer spectra at T = 5 - 15 K (Figure 2B). First-principles calculations on $MnCp_2$ molecule, which has the same number of 3d electrons as the amino-ferrocene molecule, gives a magnetic anisotropy of about 0.2 meV in the direction perpendicular to the planes holding the cyclopentadienyl rings in $MnCp_2$.[27] An anisotropy energy K = 0.2 meV leads to a blocking temperature T_B = 0.09 K using $T_B \approx K/25k_B$.[19] This temperature is much lower as compared to the onset temperature (≈ 15 K) in the splitting (Figure 2B). Thus, magnetic anisotropy is not at the origin of this splitting. Furthermore, from the electronic and geometric structures of the ferrocene molecule[28,29] and from the arrangement of amino-ferrocene molecules within the nanocluster (Figure 1A), there is no direct chemical coordination between neighboring Fe ions, suggesting that the bond-mediated interactions between Fe ions are weak to explain the properties generated at $T \lesssim 15$ K. Therefore, the splitting originates from magnetic dipole interactions between Fe ions densely arranged within a nanocluster.

We can also represent the distribution of spin orientations at Fe ion sites within the nanocluster by using an assembly of classical spins at the positions of Fe ions within a given nanocluster (**Figure 3**A). The lateral distance between neighboring Fe ions was taken as the experimental value (0.28 nm).[9] The vertical distance was assumed to be 0.4 nm, which is 20 % longer than the distance between two cyclopentadienyl rings of a given ferrocene molecule (0.33 nm).[29] We assumed that these localized spins have classical magnetic moments of 5 μ_B. Magnetic screening[30] and magnetic interactions through spin-polarized carriers[31] are negligible due to the insulating GO nanosheet. A zero-field Markov-chain Monte Carlo simulation[32] of the assembly shows that there is a monotonic decrease in the average total dipole energy with decreasing temperature (Figure 3B). The snapshots of spin orientations and dipole energy at the sites are shown in Figure 3C-F. The vortex structure of spin orientations was formed at T = 0.01 K by minimizing the dipole energy while reducing the thermal perturbations. As the temperature increases, the structure becomes thermally perturbed, and the the low dipole energy regions (colored by red, orange, and sand in Figure

3C-F) become smaller in lateral size. The energy change is due to the formation of the *entangled structures* of the spin orientations in such a way that the total dipole energy is reduced. The term *"entangled structure"* refers here to the "entangled polymers" below the glass transition temperature.[33] At T < 0.2 K, vortex structures of the spin orientations are formed. At $T \gtrsim 0.2$ K, spatially entangled structures of the spin orientations are formed, and they are simply estimated by the size of the low dipole energy regions. Note that there is here a large change in the total dipole energy at $T \lesssim 15$ K (Figure 3B) consistent with the temperature at which splitting started in the Mössbauer spectra (Figure 2B).

The model simulation elucidated several magnetic properties generated by the dense stacking of weakly interacting molecular spins in the nanocluster. The magnetization M_{AFc} of the molecule in AFc-GO sheets ($\langle d \rangle$ = 10 nm) under a static magnetic field was well fitted by an average magnetization calculated for the assembly in the field region (1 kOe $\lesssim H \lesssim$ 5 kOe), where the applied field is comparable to the magnetic dipole fields within the nanocluster (**Figure 4**A). The deviation of the data from the Brillouin curves with S = 5/2 in Figure 1C is mainly caused by the interactions between the spin orientations. In addition, this entanglement acts to resist spin alignment in the direction of the field, producing a negative Θ in the Curie-Weiss law (Figure 1D). Simulation of an assembly (S = 5/2) with vertical distance l_v of 0.20, 0.21, and 0.25 nm showed a large decrease in the average dipole energy at $T \lesssim 15$ K (Figure 4B). It should be noted that the dipole energy of an assembly (l_v of 0.2 nm) composed of magnetic moments of 1 μ_B (S = 1/2) did not change at $T \gtrsim 2$ K (Figure 4B), confirming that large magnetic moments of the molecules play an important role in the substantial decrease of the energy at $T \lesssim 15$ K. Since the thermal fluctuations of the spin orientations are weakened by the entangled structure of the spin orientations, the temperature at which the spin fluctuations are strongly reduced is similar to the temperature at which the dipole energy is strongly reduced by the formation of the entangled structures (Figure 4C).

The model simulations also revealed features characterizing the stability of the spin orientation distribution in the assembly. The spin orientations and dipole energy at the sites at T = 0.01 K were nearly the same regardless of the Monte Carlo steps (MCS) (Figure 4D), indicating that this entangled structure, namely the vortex structure, was stable. As the temperature increased, the site distribution of spin orientations and dipole energy changed against the progress of the MCS (Figure 4E,F), keeping the total dipole energy close to the average value. The low dipole energy domain (colored by red, orange, and sand in Figure 4E,F) was formed by minimizing the energy. As the simulation progressed, the domain

frequently changed its position within the nanocluster at T = 0.5 and 10 K (Figure 4E, F) and behaved like a liquid, suggesting that there are many possible spin orientation distributions in the assembly with the same energy (Figure S4, Supporting Information). This is similar to many degenerate states in spin-glass materials [14,15] and spin liquid states in frustrated magnets.[16,17] As the temperature was further increased, sites with a low or high dipole energy were distributed almost in isolation and changed the positions frequently (Figure S4B, Supporting Information).

At low temperature, magnetic dipole interactions in the dense stacking of molecular spins in the nanocluster give rise to two characteristic phenomena: spin correlations and slow dynamics. For AFc-GO sheets with $\langle d \rangle$ = 10 nm, the imaginary component χ''_{AFc} of the dynamic susceptibility of the molecule emerged at $T \lesssim$ 11 - 12 K (**Figure 5**A). From the fluctuation-dissipation theorem,[34] this suggests that spin correlations occur in this temperature range. Since there is no imaginary component for the dynamic susceptibility of pristine GO nanosheets (Figure S5, Supporting Information), these correlations occur within the nanocluster. The spin correlations are due to the magnetic interactions between the molecular spins (Figures 3B-D), which are maintained for a long time due to magnetic friction,[35] an effect neglected in the simulation. The field-cooled (FC) and zero-field-cooled (ZFC) static susceptibility $\chi_{\mathrm{M,AFc}}(T)$ curves of the AFc-GO sheets ($\langle d \rangle$ = 10 nm) separate at a temperature below the blocking temperature T_{B} of about 11 K (Figure 5B), indicating the onset of a slow magnetization relaxation analogous to that found in spin glass materials,[14,15] ferromagnetic particles[12,19] and single-molecule magnets.[36] The frequency-dependent χ'_{AFc} (Figure 5A) is typical of a slow dynamics.[14] The origin of this slow dynamics in our AFc-GO sheets results from a competition between the formation of the entangled structures by magnetic dipole interactions and their destruction by thermal perturbations. Although the dipole interaction between the nearest spins in the nanocluster is equivalent to 0.7 K, the contributing dipole interactions of all spins, which are connected due to the short intermolecular distance and the magnetic moment of 5 μ_{B}, generate the entangled structures of spin orientations essentially at $T \lesssim$ 15 K (Figure 3B). In the Mössbauer spectra (Figure 2B), the hyperfine splitting at $T \lesssim$ 15 K also originates from these slow dynamics because the relaxation time of the magnetization at $T \lesssim T_{\mathrm{B}}$ is much longer than the response time of Mössbauer spectroscopy (10^{-8} - 10^{-12} s).[22]

The relaxation process was further analyzed to extract the parameters characterizing non-equilibrium relaxation of weakly interacting spins in the nanocluster. The residual

magnetization $M(t)$ of AFc-GO sheets ($\langle d \rangle$ = 10 nm) was generated by the removal of the field after field-cooling (500 Oe) to each temperature and decayed slowly (Figure S6A, Supporting Information). Field-cooling of AFc-GO sheets forced the spin orientations to align with the direction of the field. The removal of the field caused a non-equilibrium distribution of spin orientations observed as the residual magnetization. The relaxation process was analyzed using a stretched exponential form:[14,37] $M(t) = M(0)\exp\left[-(t/\tau)^{1-n}\right]$, where τ is the relaxation time, $M(0)$ is the residual magnetization, and $0 \leqq n \leqq 1$. Fitting the data yielded a relaxation time $\tau(T)$ as a function of temperature and n of about 0.67. This relaxation time is assumed to follow a classical thermal activation process, i.e., an Arrhenius process:[14,38] $\tau(T) = \tau_0 \exp\left[E_{\mathrm{A,FC}}/k_{\mathrm{B}}T\right]$, where τ_0 is a prefactor characterizing the relaxation time scale and $E_{\mathrm{A,FC}}$ is the height of the energy barrier blocking the decay of the residual magnetization for field-cooled AFc-GO sheets. A linear fit of the plot $ln(\tau(T))$ versus T (Figure 5C) supports this assumption, yielding $E_{\mathrm{A,FC}}/k_{\mathrm{B}}$ = 11 K and τ_0 = 1.6 × 10^4 s. The strength of the energy barrier that maintains the residual magnetization against thermal activation is equivalent to the degree of spatial entanglement of the spin orientations.

The two processes: the alignment of spins by the applied magnetic field and the subsequent removal of the field to create a non-equilibrium spin orientation distribution were applied to AFc-GO sheets ($\langle d \rangle$ = 10 nm) after zero-field-cooling (ZFC). By applying the field to the zero-field-cooled sheets for 2 h, the random distribution of the spin orientations after the ZFC was changed to the distribution whose spin orientations were partially aligned with the direction of the applied field. Removal of the field caused spin orientations in the non-equilibrium distribution, resulting in a residual magnetization that slowly decayed (Figure S6B, Supporting Information). Its relaxation was analyzed by the same method applied to the field-cooled sample (Figure S7, Supporting Information). The blocking energy barrier $E_{\mathrm{A,ZFC}}/k_{\mathrm{B}}$ ($\lesssim$ 4 K) and the residual magnetization $M(0)$ ($\lesssim$ 0.08 emu/g) generated in the zero-field-cooled AFc-GO sheets were much smaller than $E_{\mathrm{A,FC}}/k_{\mathrm{B}}$ (= 11 K) and $M(0)$ (~0.15 emu/g) of the field (500 Oe)-cooled sheets (Figure 5D), indicating the difference in the number of molecules forming the entangled structures within the nanocluster. Note that $E_{\mathrm{A,ZFC}}$ depends on the field applied after ZFC (Figure 5D). A larger magnetic field applied to the zero-field-cooled AFc-GO sheets induces a larger number of spins to align their orientations with the direction of the field, resulting in a larger deviation from the random distribution and, consequently, a higher energy barrier after removal of the field. This result demonstrates that the non-equilibrium distribution and the residual magnetization, namely, the entangled

structures of the spin orientations in the nanocluster can be tuned by varying the intensity of the applied field for the AFc-GO sheets whose spin orientations are randomly distributed.

3. Conclusions

This study shows that weakly interacting molecular spins in a nanocluster with an average diameter of about 2 nm behave like a spin liquid, which is confirmed by the results that the present system exhibits slow dynamics and spin correlations below the blocking temperature and that the spin orientation distribution has so many degenerate states. Analysis of the Mössbauer spectrum and magnetic susceptibility shows that the magnetic state of the Fe ions in the nanocluster is in the 5/2 high-spin state. The creation of unique functionalities such as slow dynamics, spin liquid-like behavior, and tunable non-equilibrium spin orientation distribution in 2 nm space on a surface provides new insights into low-dimensional magnetism and spintronics. The design and synthesis of chemically functionalized nanosheets by arranging magnetic molecules through on-surface chemistry will lead to major advances in the development of 2D materials and 2D spintronic devices.

4. Methods

Chemical synthesis: One mL of GO solution (4 mg/mL) was mixed with 50 mL of *N*,*N*-dimethylformamide (DMF) in a round-bottomed flask. The solution was stirred while adding amino-ferrocene powder (20 mg) and coupling agents (EDC-HCl, HOBt and trimethylpyridine) at 0 ˚C for the first 3 hours to reduce the overreaction, and then stirred at 24 ˚C for 4 hours. The on-surface chemical reaction produced amino-ferrocene-based nanoclusters with an average inter-cluster distance of 10 nm on the GO nanosheet. The as-synthesized products were separated from the supernatant liquid by using an ultrafast centrifuge after repeated washing first twice with DMF and then with ethanol to remove unreacted chemicals on the sheets, followed by drying.

Magnetization measurement: The static magnetization M of aggregated AFc-GO sheets weighting 5-30 mg was measured using a superconducting quantum interference device (SQUID) magnetometer (MPMS-7T, Quantum Design). The static magnetic susceptibility $\chi_{\mathrm{M,AFc}}$ was calculated as $\chi_{\mathrm{M,AFc}} = M_{\mathrm{AFc}}/H$ by using the applied static magnetic field H. The dynamic susceptibility was measured at zero static magnetic field by using a SQUID magnetometer (MPMS-1T, Quantum Design) at an alternating field (amplitude ΔH = 1 or 0.5 Oe) with driving frequency f = 2 - 500 Hz. The slow dynamics

of AFc-GO sheets ($\langle d \rangle$ = 10 nm) was estimated by measuring the residual magnetization obtained by removing the field after the sheets were slowly cooled to the temperature under the field of 500 Oe. The residual magnetization of the zero-field-cooled sheets was obtained by the following three steps: 1) zero-field-cooling slowly to a target temperature; 2) applying a magnetic field for 2 hours at the temperature; 3) removing the field at each temperature. The change in the residual magnetization was then measured as a function of time at each temperature. Mössbauer spectroscopic measurements were performed using a conventional transmission geometry with the ^{57}Fe excitation energy of 14.4 keV to see the magnetic states of the Fe ions in the AFc-GO sheets. The source velocity was calibrated using pure α-Fe films. A sample with a diameter of about 14 mm was formed by random stacking of AFc-GO sheets, and it was dried and covered with thin Kapton sheets. For the measurements, the sample was sandwiched between thin pure Al films to keep the temperature distribution uniform. The sample with a total weight of Fe atoms of about 20 mg was placed on a stage of a low-temperature cryostat. The spectra were fitted with magnetically-split sextets with Voigt profiles (convolution of Lorentzian and Gaussian functions) and non-magnetic doublets with Lorentzian functions profiles.

Markov-chain Monte Carlo simulation: The Monte Carlo algorithm generated a sequence of spin orientations as follows. (1) The initial state of the assembly (Fig. 3a) was a spin configuration where each spin orientation was random. (2) The program randomly selected a molecular site within the assembly and changed its spin orientation to the direction denoted by θ and φ in polar coordinates ($0 \leqq \theta \leqq \pi$ and $0 \leqq \varphi \leqq 2\pi$) by using random numbers. After calculating the energy difference ΔE between the spin configurations before and after the spin orientation change, the Boltzmann factor $\exp(-\Delta E/k_{\mathrm{B}}T)$, where k_{B} is the Boltzmann constant and T is the temperature of the assembly, was used to estimate the probability P of the spin orientation change according to a Markov chain process. (3) The program randomly selected a fraction R with equal probability over the interval [0,1]. Then it performed the orientation change if $R \leq P$, where P is calculated as $P = x/(1+x)$; $x = \exp(-\Delta E/k_B T)$. After repeated iterations of steps (2) and (3), the system was at or near equilibrium. This method is called the heat-bath method.[28] The initial configurations (600 Monte Carlo steps (MCS)) in the simulation were removed for the calculation of the average value, because the configurations were out of thermodynamic equilibrium.

Supporting Information

Supporting Information is available from the Wiley Online Library or from the author.

Acknowledgements
We thank Prof. K. Mibu of Nagoya Institute of Technology and Prof. E. Kita of Tsukuba university for the insightful discussion. The Mössbauer spectroscopic measurements were performed under the Nanotechnology Platform Program of MEXT, Japan. This work was supported by JSPS KAKENHI Grant Number JP21K0482, Grand-in-Aid for User Facility Service in NIMS, and by the International Center of Materials Nanoarchitectonics (WPI-MANA), MEXT, Japan.

Conflict of Interest
The authors declare no conflict of interest.

Data Availability Statement
The data that support the findings of this study are available from the corresponding author upon reasonable request.

Keywords
Amino-ferrocene, magnetic dipole interaction, entangled structure, nanocluster, graphene oxide, slow dynamics, 2D material

Received: ((will be filled in by the editorial staff))
Revised: ((will be filled in by the editorial staff))
Published online: ((will be filled in by the editorial staff))

References

[1] J. S. Miller and A. J. Epstein, *Ang. Chem. Int. Ed. Engl.* **1994**, *33*, 385.
[2] L. F. Chibotaru, *Molecular Nanomagnets and Related Phenomena* (Ed. S. Gao, Splinger, 201) 185.
[3] N. Ishikawa, M. Sugita, T. Ishikawa, S. Koshihara, Y. Kaizu, *J. Am. Chem. Soc.*, **2003**, *125*, 869.
[4] F. S. Guo1, B. M. Day, Y. C. Chen, M. L. Tong, A. Mansikkamäki, R. A. Layfield, *Science* **2018**, *362*, 1400.
[5] L. Bogani, W. Wernsdorfer, *Nature Mat.* **2008**, *7*, 179.
[6] A. G. Arino, F. Luis, S. Hill, E. Coronado, *Nature Chem.* **2019**, *11*, 301.
[7] C. Cervetti, A. Rettori, M. G. Pini, A. Cornia, A. Repollés, F. Luis, M. Dressel, S. Rauschenbach, K. Kern, M. Burghard, L. Bogani, *Nature Mat*., **2015**, *15*, 164.
[8] K. Katoh, S. Yamashita, N. Yasuda, Y. Kitagawa, B. K. Breedlove, Y. Nakazawa, and M. Miyasaka, *Angew. Chem. Int. Ed.* **2018**, *57*, 9262.
[9] M. Sakurai, P. Koley, M. Aono, *J. Phys. Chem. C*, **2019**, *123*, 29679.
[10] R. H. Crabtree, The Organometallic Chemistry of the Transition metals (Wiley, **2014**) chap. 5.
[11] J. L. Dormann, D. Fiorani, E. Tronc, *Advances in Chemical Physics,* **1997**, *98*, 283.
[12] D. Farrell, Y. Cheng, R. W. McCallum, M. Sachan, S. Majetich, *J. Phys. Chem. B*, **2005**, *109*, 13409.

[13] P. Panissod and M. Drillon, *Magnetism: Molecular to Materials IV* (Ed. J. S. Miller and M. Drillon, Wiley-VCH Verlag GmbH & Co, 2002) Chap 7.
[14] J. A. Mydosh, *Spin glasses: an experimental Introduction* (Taylor & Francis, **1993**) chap. 3.
[15] K. Binder, A.P. Young, *Rev. Mod. Phys.* **1986**, *58*, 801.
[16] L. Balents, *Nature* **2010**, 464, 199.
[17] C. Nisoli, R. Moessner, P. Schiffer, *Rev. Mod. Phys.* **2013**, *85*, 1473.
[18] O. Kahn, *Molecular Magnetism* (VCH, **1992**) chap 2.
[19] A. P. Guimarães, *Principles of Nanomagnetism* (Springer, **2009**) chap. 3.
[20] A. Bino, D.C. Johnston, D.P. Goshorn, T.R. Halbert, E. I. Stiefel, *Science*, **1988**, *241*, 1479.
[21] S. Rajca, A. Rajca, J. Wongsriratanakul, P. Butler, S. Choi, *J. Am. Chem. Soc.*, **2004**, *126*, 6972.
[22] P. Gütlich, R. Link, A. Trautwein, *Mössbauer spectroscopy and Transition Metal Chemistry* (Springer-Verlag, **1978**) chap. 6.
[23] N. N. Greenwood, T. C. Gibb, *Mössbauer Spectroscopy* (Chapman and Hall Ltd, **1971**) chap 3.
[24] S. Mørup, H. Topsøe, *Appl. Phys*., **1976**, *11*, 63.
[25] L. F. Chibotaru, *Molecular Nanomagnets and Related Phenomena* (Ed. S. Gao, Springer, **2015**) 185.
[26] S. Chikazumi, *Physics of Magnetism* (John Wiley & Sons, Inc. **1964**) chap 7.
[27] K. Nawa, Y. Kitaoka, K. Nakamura, T. Akiyama, T. Ito, *J. Appl. Phys.*, **2015**, *117*, 17E131.
[28] A. Haaland, *Acc. Chem. Res*., **1979**, *12*, 415.
[29] C. L. Perrine, M. Zeller, J. Woolcock, A. D. Hunter, *J. Chem. Crystllogr.*, **2005**, *35*, 717.
[30] M. Koshino, Y. Arimura, T. Ando, *Phys. Rev. Lett.*, **2009**, *102*, 177203.
[31] A. H. C. Neto, F. Guinea, N. M. R. Peres, K. S. Novoselov, A. K. Geim, *Rev. Mod. Phys*., **2009**, *81*, 109.
[32] K. Binder, D. W. Heermann, *Monte Carlo Simulation in Statistical Physics* (Springer, **2010**) chap. 1, 2.
[33] R. S. Porter, J. F. Johnson, *Chem. Rev*., **1966**, *66*, 1.
[34] R. Kubo, M. Toda, N. Hashizume, *Statistical Physics Ⅱ* (Springer, **1991**) chap. 1.
[35] R. Skomski, *Simple Models of Magnetism* (Oxford, **2008**) chap. 6.
[36] D. Gatteschi, R. Sessoli, J. Villain, *Molecular Nanomagnets* (Oxford, **2010**) chap. 4.
[37] R. G. Palmer, D. L. Stein, E. Abrahams, P. W. Anderson, *Phys. Rev. Lett.*, **1984**, *53*, 958.

[38] S. Bedanta, O. Petracic, W. Kieemann, *Handbook of Magnetic Materials*, **2015**, *23*, 1.

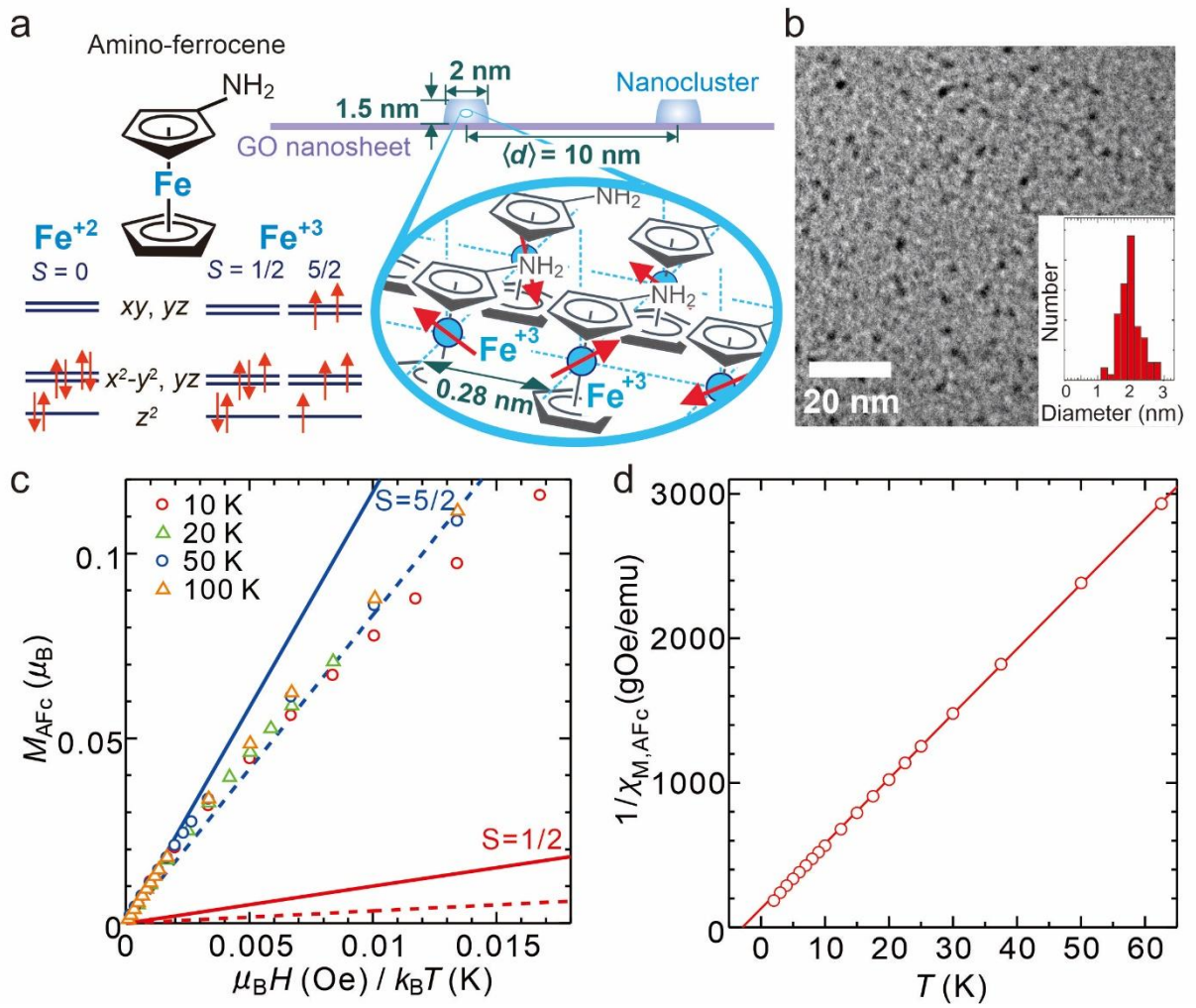

Figure 1 (a) Schematic illustration of an amino-ferrocene molecule, approximate energy splitting of the 3d orbitals in the Fe^{2+} (S = 0), Fe^{3+}(S = 1/2), and Fe^{3+} (S = 5/2) ions of a ferrocene unit, and schematic drawing of a nanocluster consisting of amino-ferrocene molecules with an average inter-cluster distance $\langle d \rangle$ of 10 nm on a graphene oxide (GO) nanosheet. (b) A transmission electron microscope (TEM) image of an AFc-GO sheet ($\langle d \rangle$ = 10 nm). The inset shows the diameter distribution of the AFc-GO sheets.(c) Magnetization M_{AFc} of molecules of AFc-GO sheets ($\langle d \rangle$ = 10 nm), Brillouin function (solid lines), and Langevin function (dotted lines) plotted against $\mu_{\mathrm{B}}H/k_{\mathrm{B}}T$. (d) Inverse of the static susceptibility of the molecule $\chi_{\mathrm{M,AFc}}$ for AFc-GO sheets ($\langle d \rangle$ = 10 nm) versus temperature. The solid line is from the Curie-Weiss law.

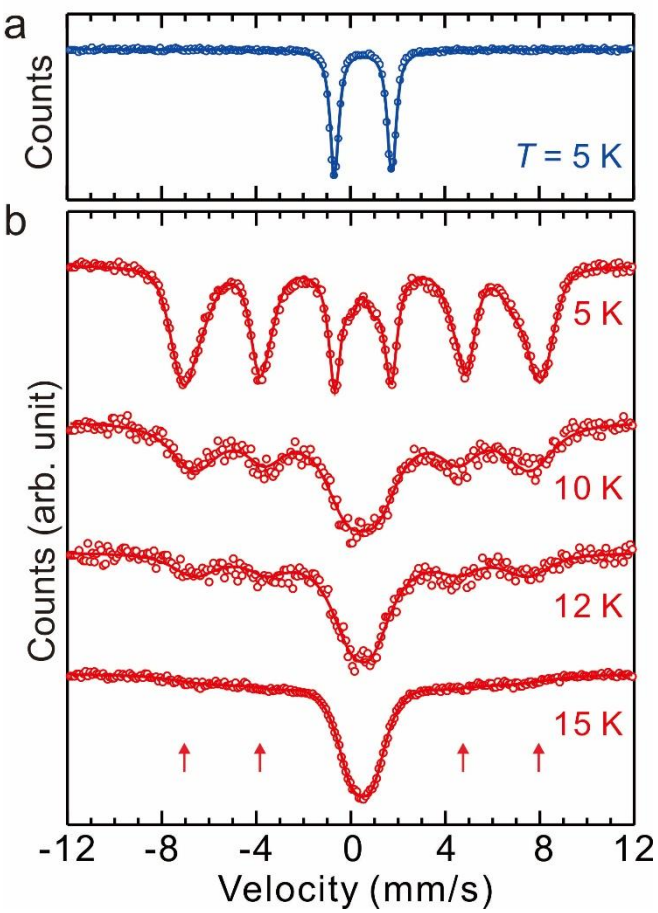

Figure 2 Mössbauer spectra of (a) pristine amino-ferrocene powder at 5 K. (b) amino-ferrocene-based nanoclusters on a graphene oxide nanosheet ($\langle d \rangle$ = 10 nm) at T = 5 – 15 K.

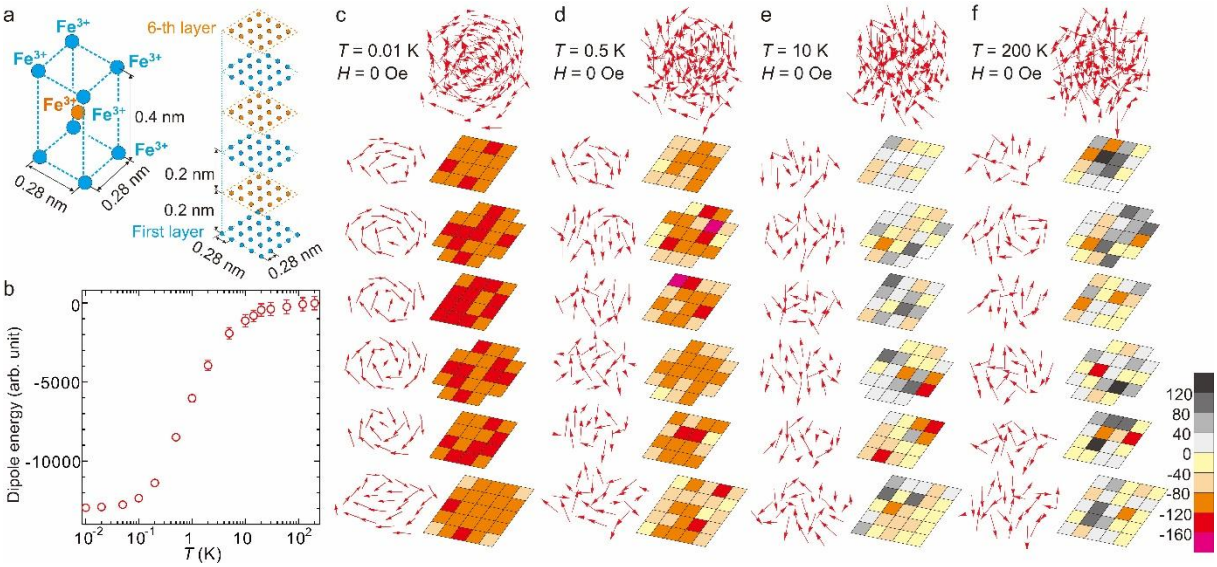

Figure 3 (a) Schematic illustration of the fundamental unit of Fe ions of amino-ferrocene molecules (left panel) and the positions of Fe ions within the nanocluster (right panel). (b) Plot of the average total dipole energy of the spin assembly, calculated using a zero-field Markov-chain Monte Carlo method, versus temperature. Snapshots of spin orientations at sites of the assembly (top), spin orientations (left), and dipole energy (right) at sites of the layers forming the assembly calculated at (c) T = 0.01 K, (d) 0.5 K, (e) 10 K, and (f) 200 K under a zero field.

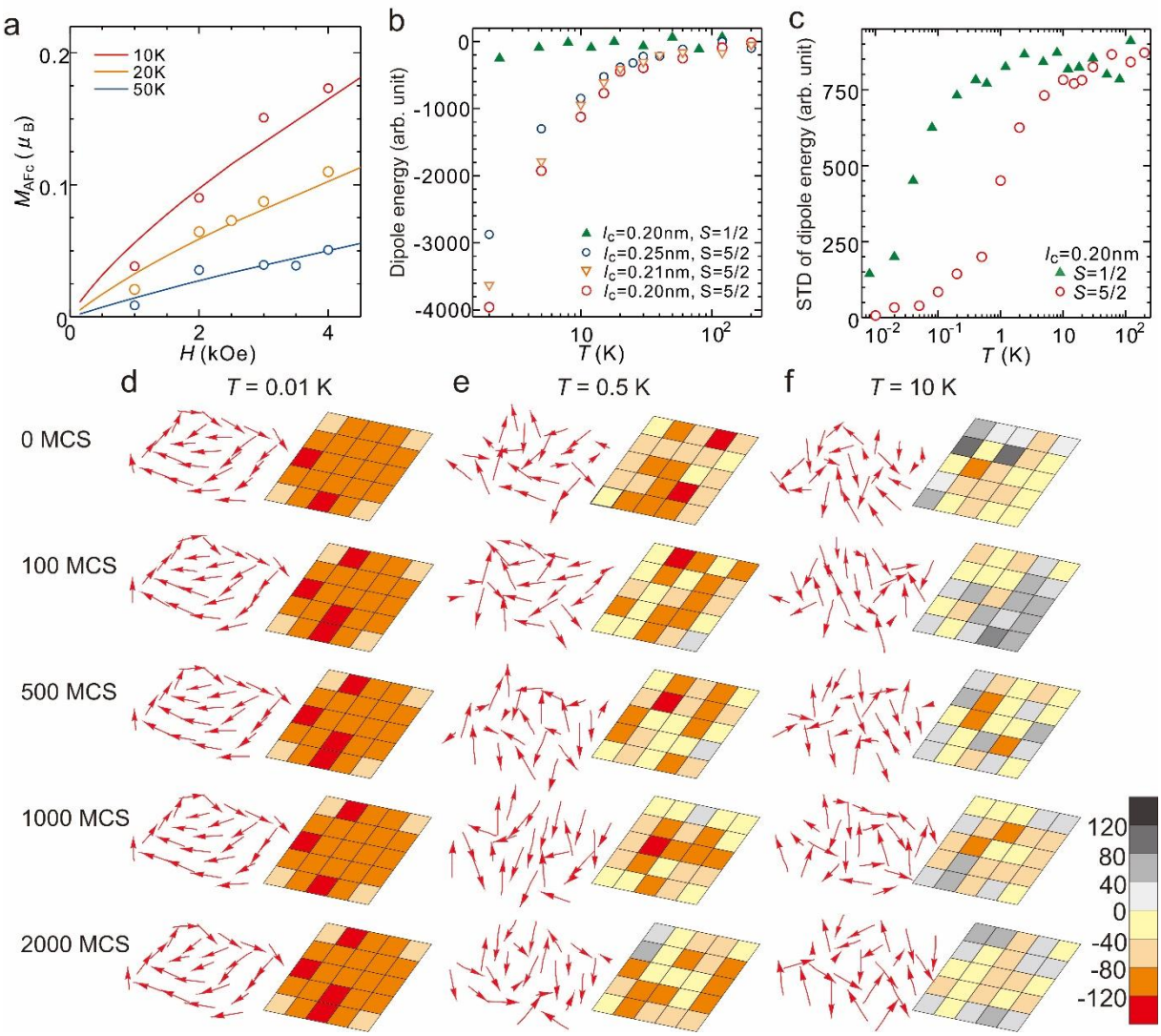

Figure 4. (a) Calculated magnetization M_{AFc} of the molecule plotted versus applied field at T = 10 K, 20 K, 50 K (open circles) compared to experimental values (solid line). (b) Average dipole energy of assemblies (l_c = 0.20, 0.21, 0.25 nm, S = 5/2) and assembly (l_c = 0.20 nm, S = 1/2) versus temperature. (c) Standard deviation (STD) of the dipole energy of the assemblies (l_c = 0.20 nm, S = 1/2, 5/2) versus temperature. Snapshots of spin orientations and dipole energy at sites of the bottom layer of the assembly (l_c = 0.20 nm, S = 5/2) versus each MCS at temperature T of (d) 0.01, (e) 0.5, (f) 10 K.

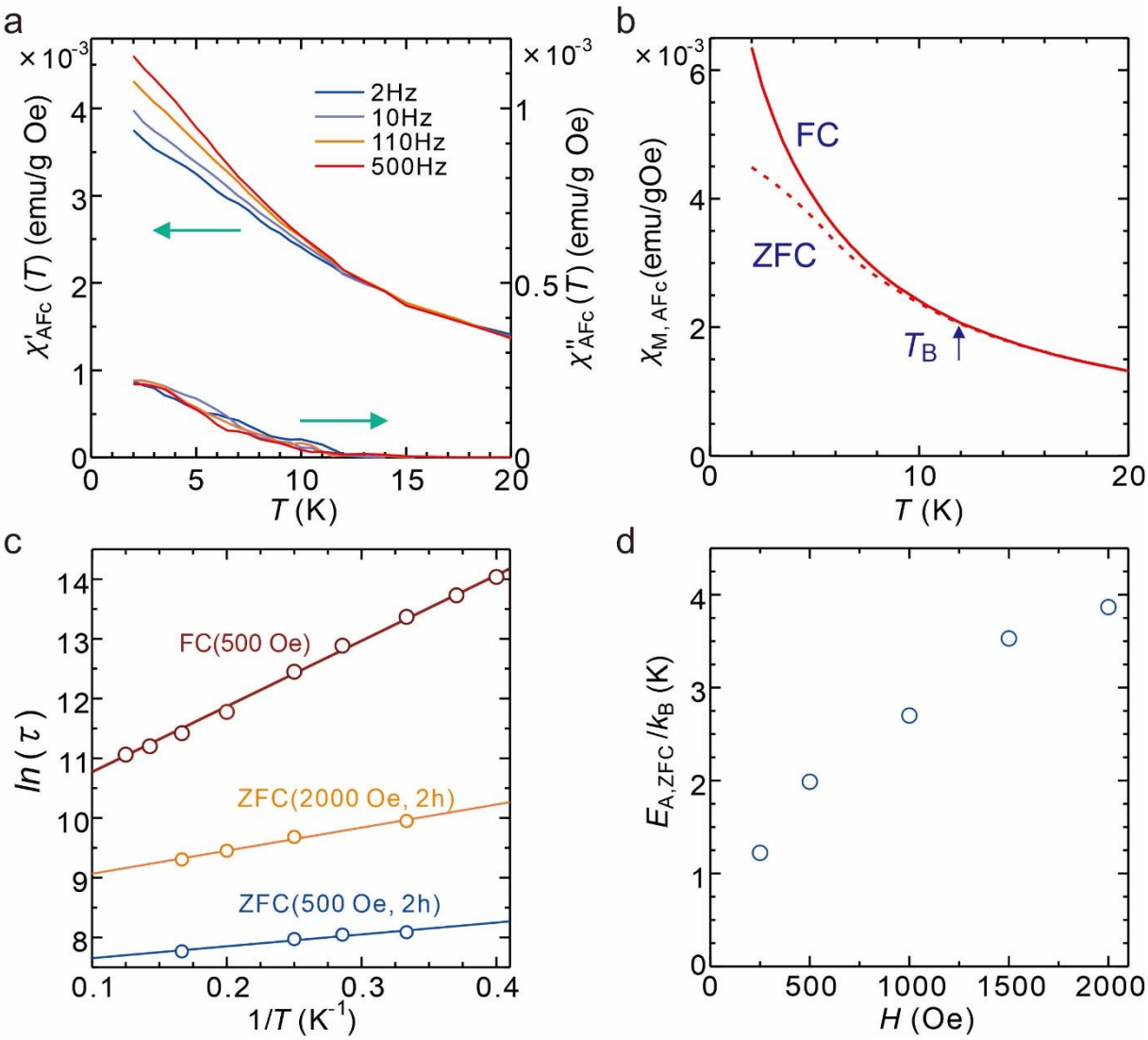

Figure 5. (a) Dynamic susceptibility (real component: χ'_{AFc}, imaginary component: χ''_{AFc}) of the molecules of AFc-GO sheets ($\langle d \rangle$ = 10 nm) as a function of temperature T. (b) Field-cooled (FC) and zero-field-cooled (ZFC) static susceptibilities $\chi_{\mathrm{M}}$of the molecules plotted against temperature, showing a separation between the curves at the blocking temperature T_{B}. (c) Logarithmic plot of the relaxation time $\tau(T)$ of AFc-GO sheets ($\langle d \rangle$ = 10 nm) in non-equilibrium spin orientations obtained after field-cooling (red open circle) and zero-field-cooling (orange and blue open circles) against the inverse of temperature. (d) Blocking energy barrier $E_{\mathrm{A,ZFC}}/k_{\mathrm{B}}$ in the relaxation of the residual magnetization by applying the static field H to zero-field-cooled AFc-GO sheets ($\langle d \rangle$ = 10 nm) for 2 hours and removing the field.

Makoto Sakurai*, Tsuyoshi Ueta, Christian Joachim

Spin liquid-like behavior of weakly interacting molecular spins in nanoclusters on a graphene oxide nanosheet

Magnetic dipole interactions in nanoclusters composed of densely packed amino-ferrocene molecules (S = 5/2) cause a spatially entangled structure of the spin orientations, leading to slow dynamics and a spin liquid-like behavior at a temperature where the magnetic anisotropy is negligible. The ability to create emergent functionalities in molecular assemblies with an average diameter of 2 nm on a surface provides new insights into 2D magnetism.

ToC figure

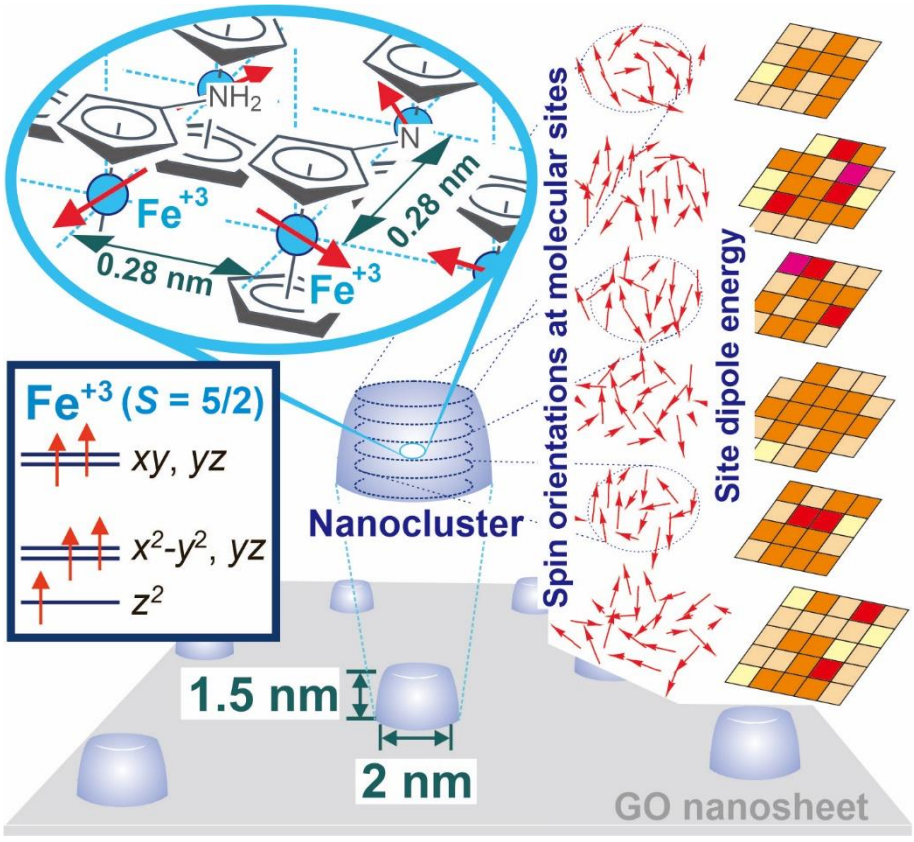

Supporting Information

Spin liquid-like behavior of weakly interacting molecular spins in nanoclusters on a graphene oxide nanosheet

Makoto Sakurai,[1] Tsuyoshi Ueta*[2] and Christian Joachim[1,3]

1 International Center for Materials Nanoarchitectonics (WPI-MANA), National Institute for Material Sciences (NIMS), 1-1 Namiki, Tsukuba, Ibaraki 305-0044, Japan
2 Jikei University School of Medicine, 8-3-1 Kokuryo, Chofu, 182-0022, Japan.
3. Centre d'Elaboration de Matériaux et d'Études Structurales (CEMES), Centre National de la Recherche Scientifique (CNRS), 29 Rue J. Marvig, BP 4347, 31055 Toulouse Cedex, France.

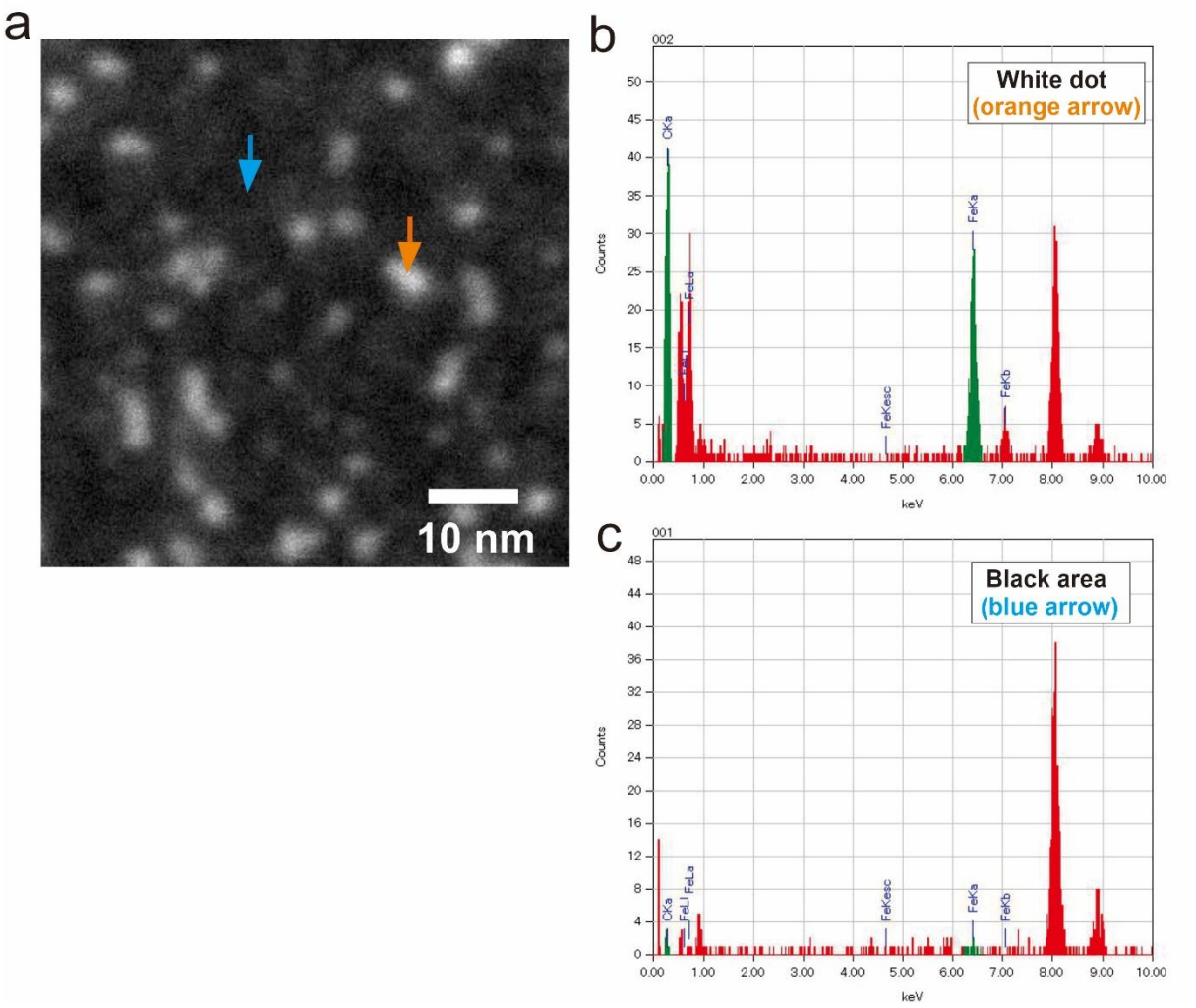

Figure S1. (a) Scanning transmission electron microscope (STEM) image of an AFc-GO sheet ($\langle d \rangle$ = 10 nm). Local EDX spectra measured for the area indicated by (b) orange and (c) blue arrows. Fe signals (Green peak at 6.4 keV) are detected only from white dots, indicating that the nanoclusters are formed from aminoferrocene molecules.

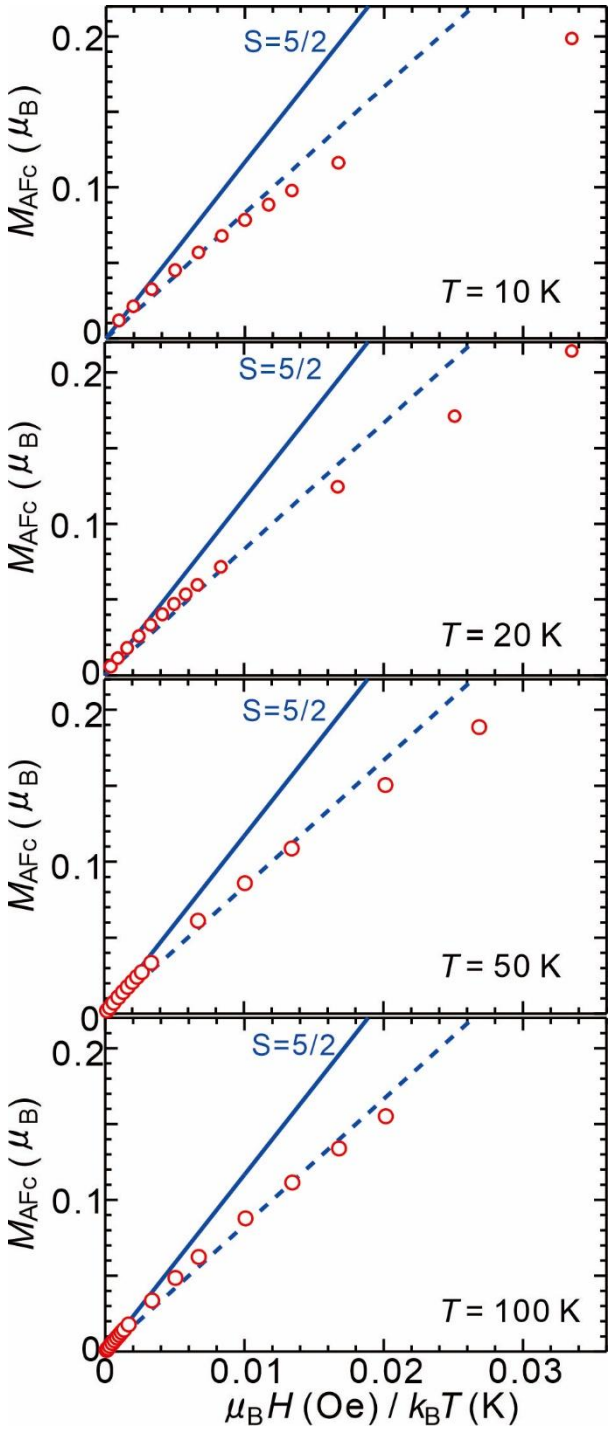

Figure S2. Magnetization M_{AFc} of the molecule within amino-ferrocene-based nanoclusters on a graphene oxide sheet (AFc-GO sheets ($\langle d \rangle$ = 10 nm)) at each temperature as a function of $\mu_B H / k_B T$. Solid and dashed lines are Brillouin and Langevin functions, respectively, with spin quantum number S = 5/2. Note that the deviation of the data from the line occurred at larger onset fields with increasing temperature.

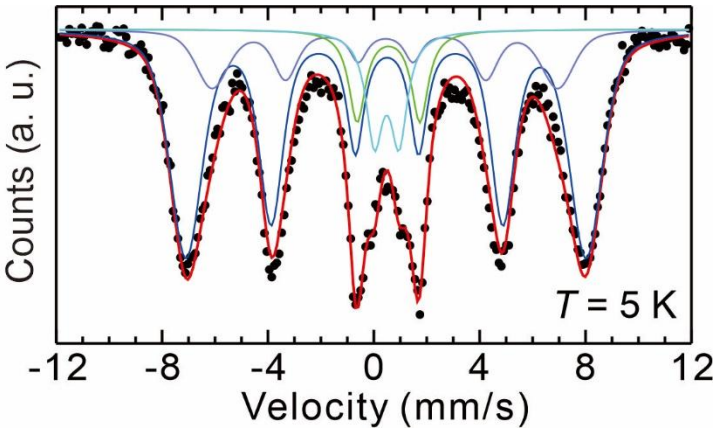

Figure S3. Mössbauer spectrum of AFc-GO sheets ($\langle d \rangle$ = 10 nm) at 5 K and fitting to the spectrum by using two magnetically split sextets with Voigt profiles (convolution of Lorentzian and Gaussian functions) and two non-magnetic doublets with Lorentzian profiles. The parameters obtained from the fit are listed in Table S1.

	IS (mm/s)	QS (mm/s)	Lorentzian width (mm/s)	HF (kOe)	Gaussian width (kOe)	Intensity ratio	Area (%)	Color
Fe (1)	0.48	-0.04	0.76	469	26	3:2:1:1:2:3	65.2	Blue
Fe (2)	0.44	-0.03	0.76	405	26	3:2:1:1:2:3	16.7	Light Blue
Fe (3)	0.56	2.37	0.76			1:1	8.3	Pink
Fe (4)	0.49	0.93	0.76			1:1	9.8	Green

IS (Chemical isomer shift), QS (quadrupole splitting), HF (Magnetic hyperfine field)

Table S1. Fitting parameters of Mössbauer spectra of AFc-GO sheets ($\langle d \rangle$ = 10 nm) at 5 K as shown in Figure S2.

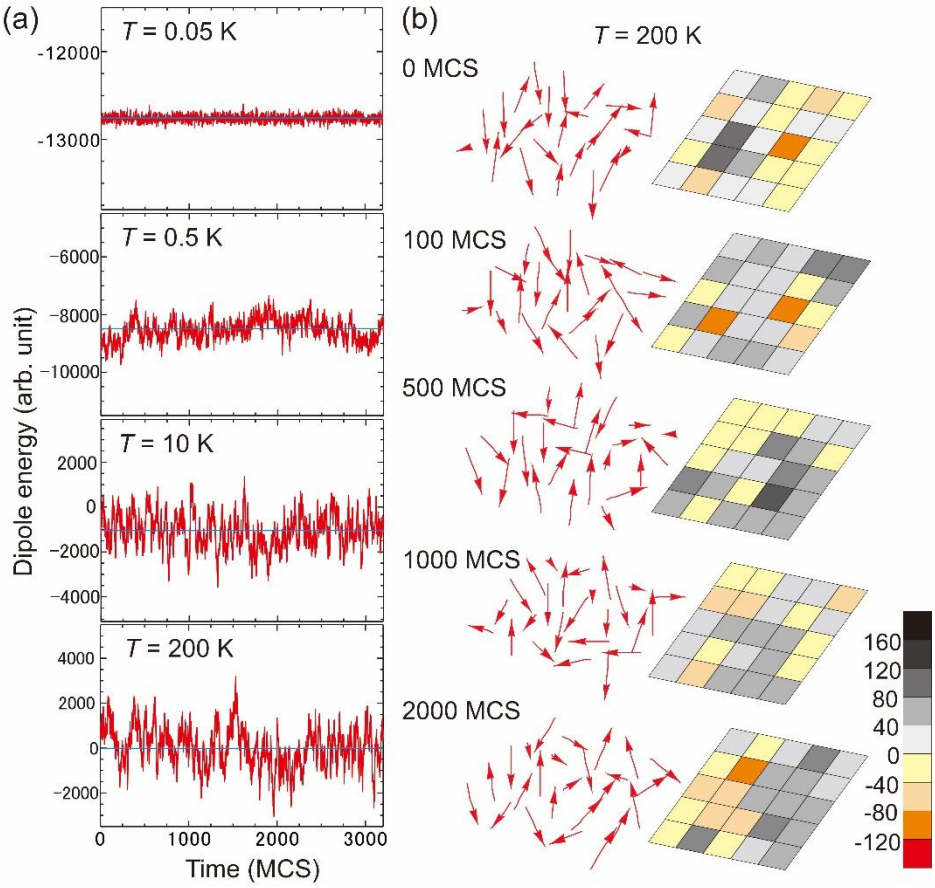

Figure S4. (a) Dipole field of the assembly versus MCS. The blue line shows the average value. (b) Snapshots of spin orientations and dipole energy at sites of the bottom layer of the assembly (l_c = 0.20 nm, S = 5/2) versus each MCS at temperature T of 200 K.

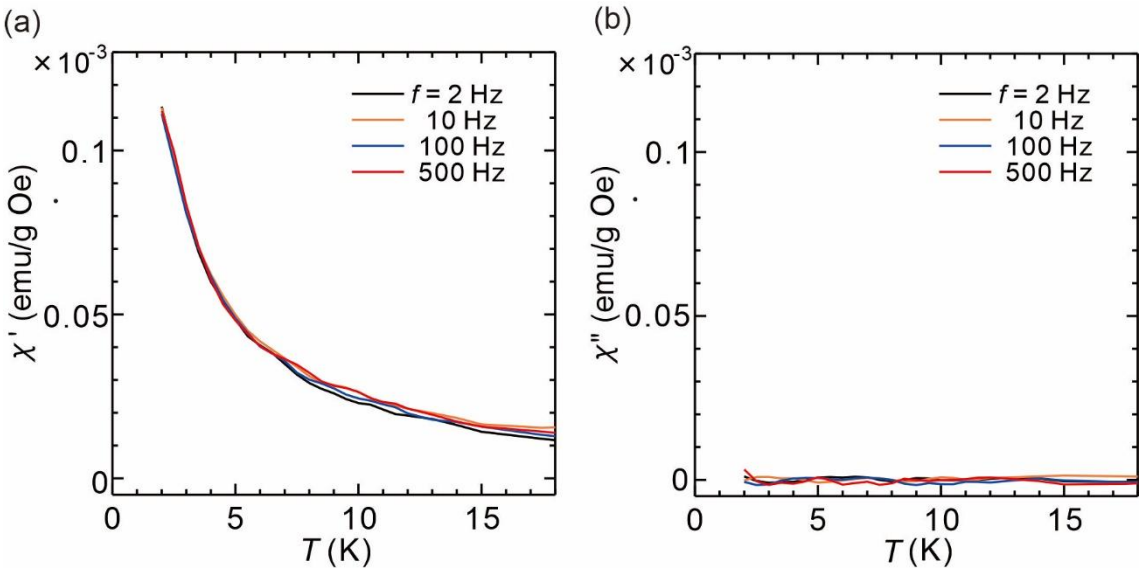

Figure S5. (a) Real χ' and (b) imaginary χ" components of dynamic susceptibility of pristine GO nanosheets at a driving frequency (f = 2, 10, 100, and 500 Hz) of the AC field (ΔH = 0.5 Oe).

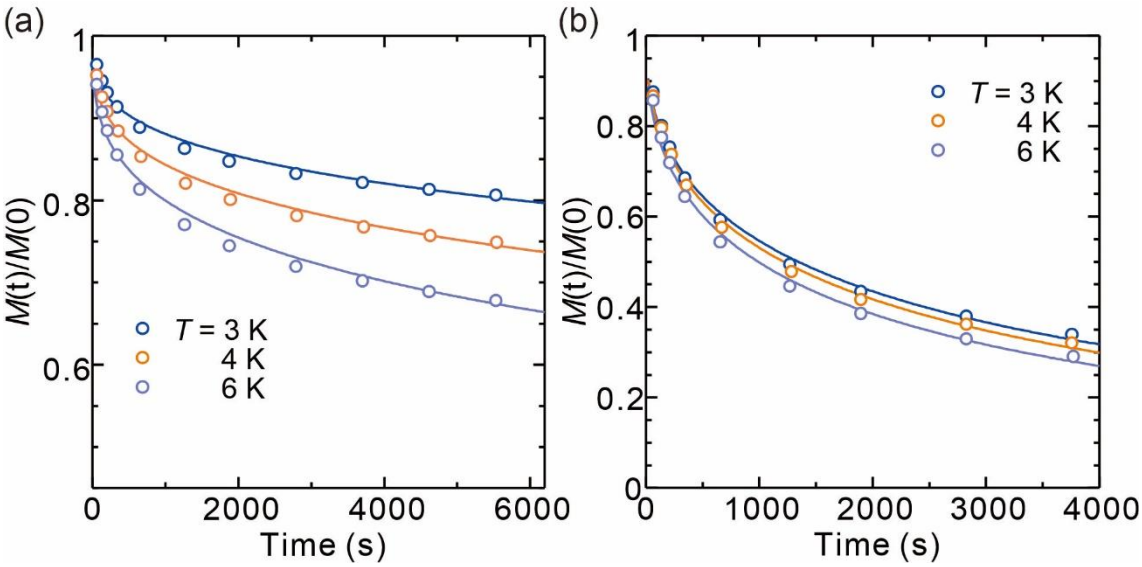

Figure S6. (a) Magnetization relaxation of AFc-GO sheets ($\langle d \rangle$ = 10 nm) after field-cooling (H = 500 Oe) and subsequent field removal. (b) Magnetization relaxation of AFc-GO sheets ($\langle d \rangle$ = 10 nm) in non-equilibrium spin orientations by the application of a static field of 500 Oe for 2 hours after zero-field-cooling to the target temperature and subsequent removal of the field at each temperature. The solid lines in (a), (b) show curves fitted to the data using the stretched exponential form.

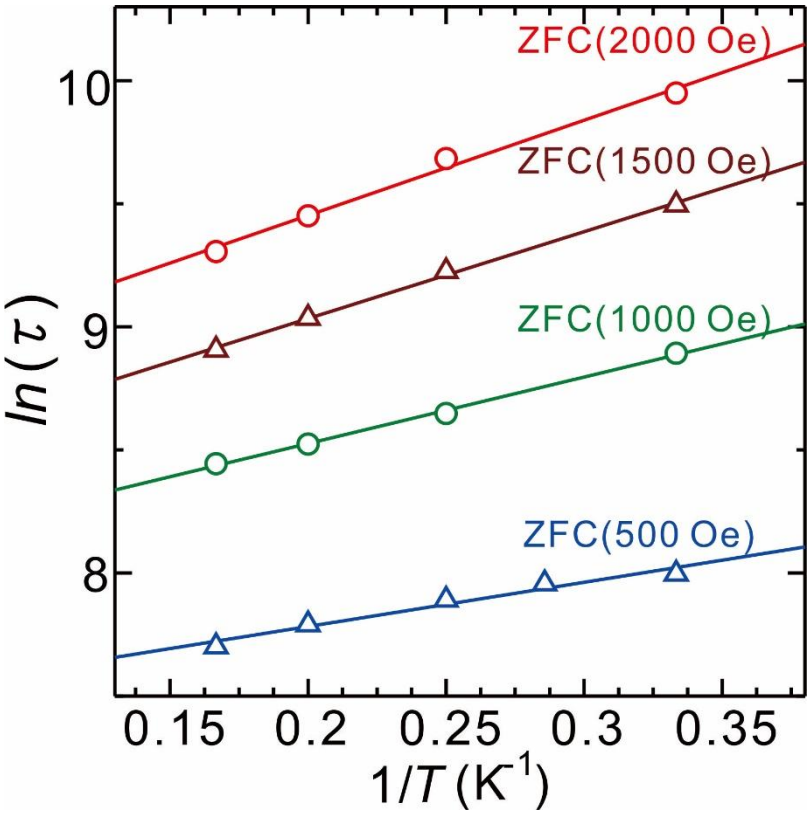

Figure S7. Logarithmic plot of relaxation time $\tau(T)$ against the inverse of temperature of AFc-GO sheets ($\langle d \rangle$ = 10 nm) in non-equilibrium spin orientations produced by the application of magnetic fields (500 – 2000 Oe) for 2 hours after the zero-field-cooling and subsequent removal of the field at each temperature.